ISSN 0020-1685, Inorganic Materials, 2018, Vol. 54, No. 3, pp. 295–300. © Pleiades Publishing, Ltd., 2018.
Original Russian Text © S.V. Shevtsov, I.A. Kovalev, A.I. Ogarkov, S.V. Kannykin, D.V. Prosvirnin, A.S. Chernyavskii, K.A. Solntsev, 2018, published in Neorganicheskie Materialy, 2018, Vol. 54, No. 3, pp. 321–326.

Structure and Hardness of Ceramics Produced through High-Temperature Nitridation of Titanium Foil

S. V. Shevtsov[a], I. A. Kovalev[a], A. I. Ogarkov[a, *], S. V. Kannykin[b], D. V. Prosvirnin[a], A. S. Chernyavskii[a], and K. A. Solntsev[a]

[a] *Baikov Institute of Metallurgy and Materials Science, Russian Academy of Sciences, Leninskii pr. 49, Moscow, 119334 Russia*
[b] *Voronezh State University, Universitetskaya pl. 1, Voronezh, 394036 Russia*
**e-mail: imet@imet.ac.ru*

Received June 3, 2017

Abstract—We have studied the variation in the phase composition, elemental composition, and microstructure of rolled titanium samples during thermal annealing in a nitrogen atmosphere at 1300, 1500, 1700, and 2000°C. The results demonstrate that the nitridation process can yield compact titanium nitride-based ceramics or TiN/TiN_x/α-Ti⟨N⟩ heterostructures. X-ray diffraction data for the near-surface region of the samples before and after nitridation and those for cross-sectional fracture surfaces of heterostructures are used to infer orientation relationships between the TiN phase and α-Ti⟨N⟩ solid solution. Scanning electron microscopy results for cross-sectional fracture surfaces indicate that complete nitridation of the samples leads to the formation of a three-layer microstructure.

Keywords: titanium nitride, ceramic, nitridation, oxidation-assisted engineering, structure, hardness, X-ray diffraction, scanning electron microscopy

DOI: 10.1134/S0020168518030135

INTRODUCTION

Titanium nitride has the inherent advantages of thermal stability, high hardness, good wear and corrosion resistances, good stability in chemically aggressive media, high thermal conductivity, and biocompatibility [1–4]. Owing to this, titanium nitride-based ceramic materials continue to attract considerable interest. Various approaches are currently used to synthesize titanium nitride, aimed mainly at producing films and coatings by various physical and chemical methods [5–9], as well as at fabricating ceramic parts by compacting and sintering appropriate powders, followed by nitridation of the resultant bodies [10–16].

An approach proposed by Kuznetsov et al. [17] for producing ceramics through complete nitridation of a metallic preform of particular shape allows one to obtain ceramic parts that are difficult to prepare by conventional ceramic processing techniques.

It follows from the phase diagram of the titanium–nitrogen system [18] that nitridation is the simplest approach for modifying the properties of the metal. As shown earlier [19], complete nitridation is possible as well above the melting point of the metal.

In this work, proceeding from the fact that the approach in question differs fundamentally from nitridation of, for example, powder compacts, we aim at gaining insight into the structural changes that accompany the complete nitridation of rolled titanium in the temperature range 1300–2000°C.

EXPERIMENTAL

The starting material used had the form of VT1-0 titanium ribbons 60 mm in length and 3.0 × 0.3 mm in cross section. The ribbons were heat-treated in an extrapure-grade nitrogen atmosphere at a pressure of $(1.2 \pm 0.1) \times 10^5$ Pa and temperatures of 1300, 1500, 1700, and 2000°C for 6, 11, 16, 21, and 60 min at each temperature. The temperature in the reactor was monitored with an ISR 50-LO pyrometer in the temperature range 700–3000°C with an accuracy of 0.5% below 1500°C and 1.0% above 1500°C.

The phase composition of the samples was determined by X-ray diffraction[1] (Thermo Scientific ARL X'TRA diffractometer, θ–θ geometry, CuK_α radiation). We used two optical schemes: classic Bragg–Brentano focusing configuration in symmetric geometry for analysis of the bulk of the samples and the parallel beam configuration (parabolic mirror + thin-film collimator) in grazing incidence mode for analysis of the near-surface region and cross-sectional fracture surfaces. The depth of the saturated layer was evaluated as $t\,(\text{mm}) = 3.45(\mu_{\text{eff}})^{-1}\sin\theta_{\max}$ [20] (where $\theta_{\max}$ is

[1] At the Shared Research Facilities Center, Voronezh State University.

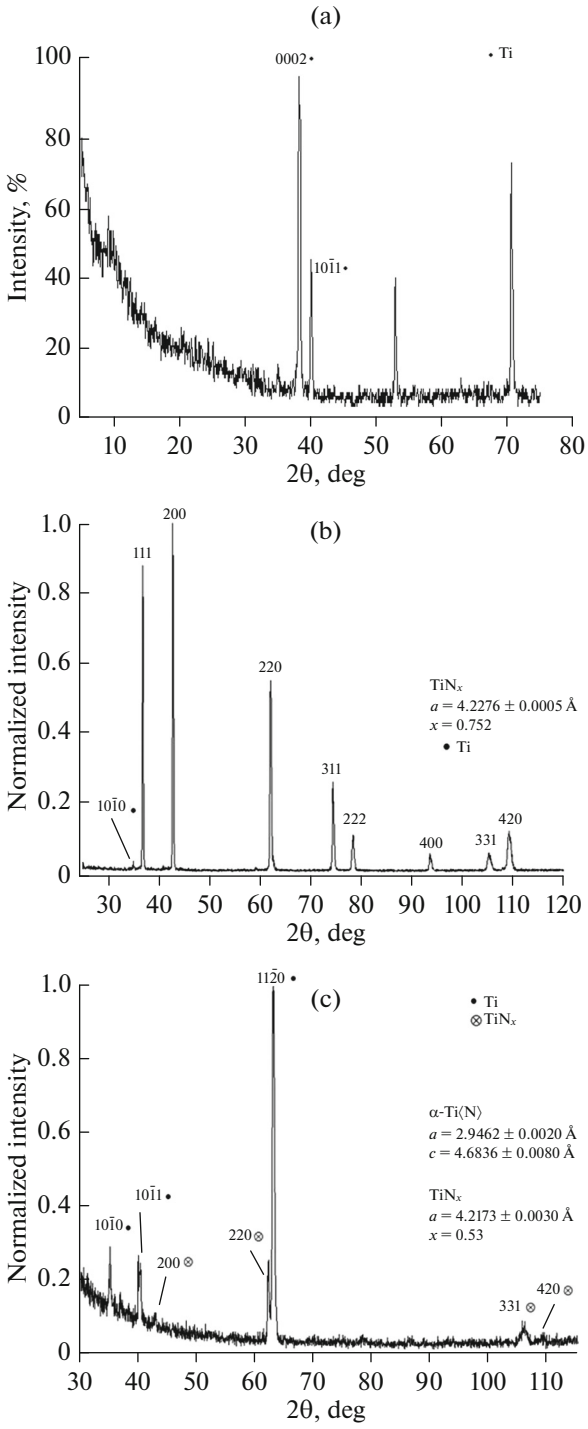

Fig. 1. X-ray diffraction patterns of the samples: (a) surface layer of the parent titanium foil; (b, c) 1300°C, 6 min; (d) 1700°C, 6 min; (e) 2000°C, 60 min; (b, e) near-surface region, (c, d) cross-sectional fracture surfaces.

the maximum angle of incidence of the X-ray beam and μ_{eff} is the linear absorption coefficient, which can be calculated from crystallographic data for TiN using the JANA2006 program [21]). In the data collection geometry used, the depth of the saturated layer ranged from 10 to 35 μm, depending on the angle of incidence

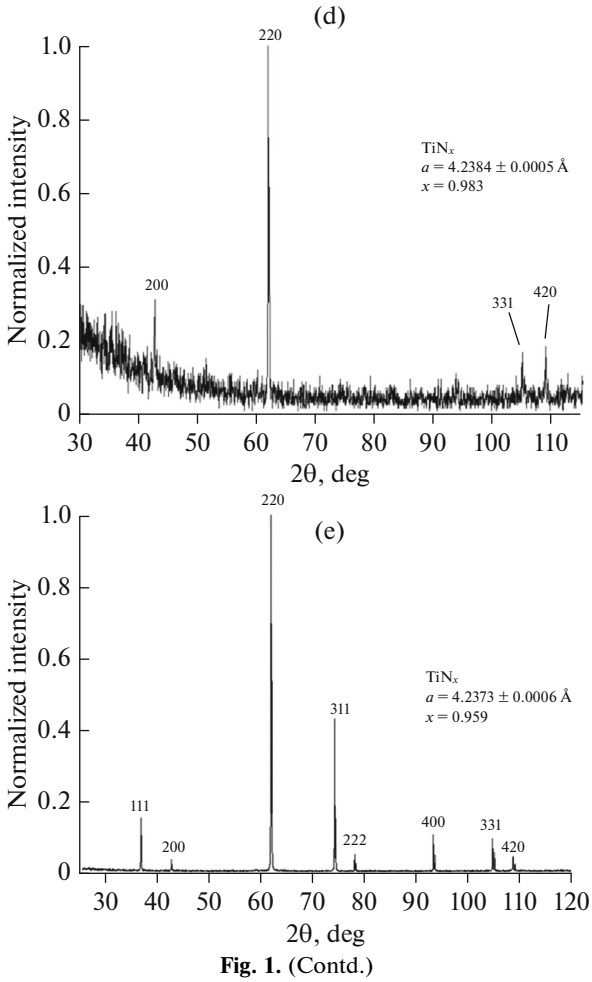

Fig. 1. (Contd.)

of the primary beam. The lattice parameter (a) of the TiN$_x$ nitride as a function of nitrogen content was determined using the equation a (Å) = 0.0467x + 4.1925 [22]. In the grazing incidence mode, the angle of incidence of the primary beam was 5° relative to the sample surface, and the data were collected while rotating the detector. The analysis depth was then 3 μm.

The surface morphology of cross-sectional fracture surfaces and the local elemental composition of the samples were studied by scanning electron microscopy (SEM) on a Carl Zeiss LEO 1420 equipped with an Oxford Instruments INCA Energy 300 energy dispersive X-ray microanalysis system.

Microhardness was measured on polished microsections of cross-sectional fracture surfaces with a Wolpert 402MVD hardness tester in conformity with the Russian Federation State Standard GOST 9450-76. The indenter used was a regular four-sided diamond pyramid with a vertex angle of 136°. The indentation load was 0.5 N and the dwell time was 10 s.

RESULTS AND DISCUSSION

Figure 1 shows X-ray diffraction patterns of the surface layer of the starting sample (Fig. 1a) and after

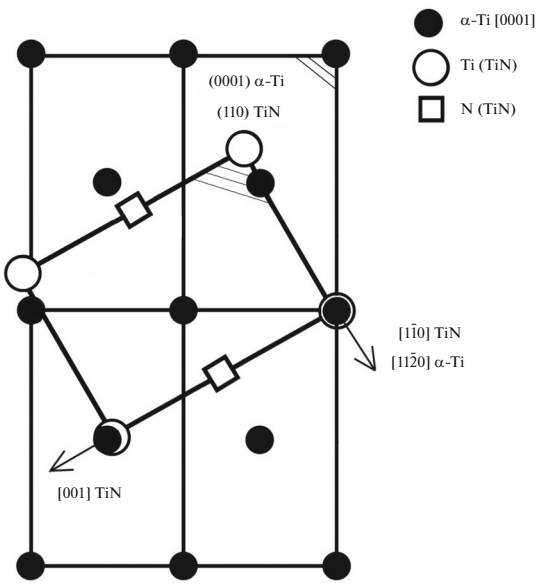

Fig. 2. Basic orientation relationship between the TiN and α-Ti according to the X-ray diffraction data in Fig. 1.

synthesis under different conditions (Figs. 1b, 1e) and those of cross-sectional fracture surfaces of the samples (Figs. 1c, 1d). It follows from the X-ray diffraction patterns in Figs. 1a, 1b, and 1e that the starting titanium samples and the α-solid solution are characterized by ⟨0002⟩ texture, whereas the titanium nitride has ⟨110⟩ texture. The X-ray diffraction patterns in Figs. 1c and 1d demonstrate that the α-Ti has a ⟨11$\bar{2}$0⟩ preferential direction, whereas the nitride has a ⟨110⟩ preferential direction. Based on the X-ray diffraction results, we obtained the following orientation relationships between the crystal lattices of the nitride and the α-Ti⟨N⟩ solid solution: (110), [1$\bar{1}$0] TiN ∥ (0001), [11$\bar{2}$0] α-Ti⟨N⟩ (Fig. 2).

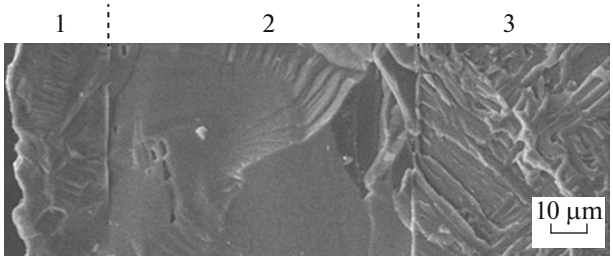

Fig. 3. SEM image of a cross-sectional fracture surface of the sample synthesized vie nitridation at 1300°C for 6 min (see text for notation).

Table 1 presents data on the variation in the elemental composition of the nitrides inferred from the present X-ray diffraction and SEM results. With increasing synthesis temperature and time, the lattice parameter of TiN_x increases, which is due to the increase in nitrogen concentration. The broadening of reflections observed in the diffraction patterns of the samples synthesized at a temperature below 1700°C may be caused by both the smaller grain size in comparison with the samples prepared at higher temperatures and a nitrogen concentration gradient across the layer analyzed. Because of this, it appears impossible in this case to evaluate the crystallite size by X-ray diffraction. In the X-ray diffraction patterns of the samples synthesized at 1700°C or a higher temperature, the full width at half maximum of the reflections is smaller and doublet splitting is observed even at small angles, which may be associated with both an increase in the grain size of the nitride and a more uniform nitrogen concentration distribution across the nitride layer [20].

The initial stage of nitridation (during the first 6 min) yields a three-layer heterostructure throughout the temperature range studied. Figure 3 shows a characteristic SEM image of a cross-sectional fracture sur-

Table 1. Effect of synthesis conditions on the lattice parameter and composition of the TiN_x samples

Synthesis conditions		a, Å	x
temperature, °C	time, min		
1 300	6	4.2276 ± 0.0005* 4.2309 ± 0.0009**	0.752* 0.820**
1 500	21	4.2279 ± 0.0005 4.2353 ± 0.0003	0.758 0.916
	60	4.2310 ± 0.0005 4.2371 ± 0.0005	0.824 0.955
1 700	60	4.2357 ± 0.0002 4.2400 ± 0.0002	0.925 1.020
2 000	21	4.2350 ± 0.0011 4.2401 ± 0.0003	0.910 1.020
	60	4.2373 ± 0.0006 4.2392 ± 0.0019	0.959 1.000

* Data acquisition in the Bragg–Brentano geometry.
** Data acquisition in grazing incidence mode.

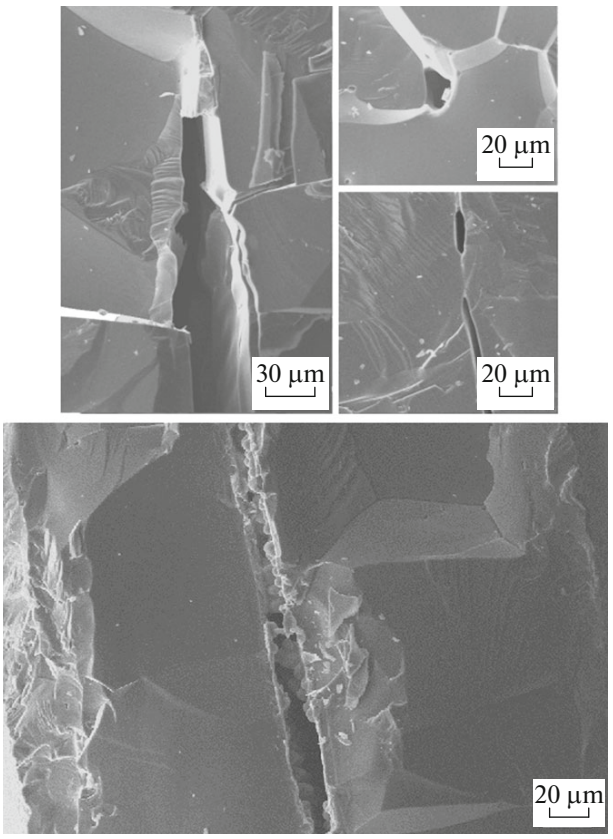

Fig. 4. SEM images of inner cavities.

face of a heterostructure synthesized vie nitridation at 1300°C for 6 min. Morphologically, there are three distinct layers differing in thickness. The thickness of the top surface nitride layer (1) is ~20 μm. The underlying nitride layer (2) is ~58 μm in thickness, and the central zone of the sample consists of a nitrogen solid solution in titanium (3). At other process temperatures, the thickness of the layers of the nitride phase increases, whereas the thickness of the solid solution

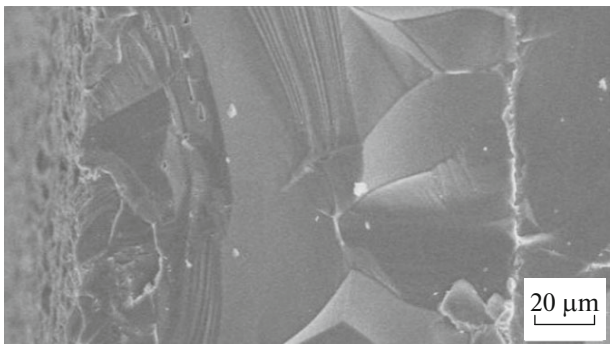

Fig. 5. SEM image of the sample synthesized at 1700°C for 30 min. The image was taken after the disappearance of the solid solution phase.

layer decreases. As a result, the formation of a bilayer structure takes 21 min at 1500°C, 16 min at 1700°C, and 6 min at 2000°C.

In the course of nitridation, the thickness of layer 3 decreases as a result of the movement of the concentration front. In this process, the solid solution phase may disappear and microcavities may form in the bulk of the material (Fig. 4). Thus, the initial stages of nitridation yield a three-layer heterostructure, whereas the result of complete nitridation after heat treatment is a single-layer structure.

Morphologically, layers 1 and 2 are separated by a boundary. The morphological distinction between the layers persists until the formation of a nitride phase close in composition to TiN, which requires 30 min of nitridation at 1500°C, 21 min at 1700°C, and 11 min at 2000°C (Fig. 5).

According to energy dispersive X-ray microanalysis data, layer 1 is uniform in elemental composition, which approaches TiN. Layer 2 has a composition gradient: in going from its surface to its central part, nitrogen content decreases (from $x = 0.94$ to 0.26).

Table 2. Microhardness measured on cross sections of the samples as a function of synthesis time at 1500, 1700, and 2000°C (the numbers 1–3 refer to forming layers revealed on cross-sectional fracture surfaces of the samples)

Synthesis time, min	Microhardness, MPa								
	1500			1700			2000		
	1	2	3	1	2	3	1	2	3
6	1649 ± 169	580 ± 35	445 ± 30	1690 ± 145	620 ± 18	470 ± 30	2003 ± 87	765 ± 61	545 ± 29
11	1600 ± 18	853 ± 144	452 ± 28	2004 ± 108	577 ± 23	498 ± 24	2136 ± 82	821 ± 75	–
16	1536 ± 78	1084 ± 113	568 ± 43	2332 ± 119	702 ± 133	–	2074 ± 82	634 ± 44	–
21	1644 ± 54	851 ± 63	–	2193 ± 108	646 ± 54	–	2103 ± 88	–	–
60	2254 ± 170	713 ± 38	–	2509 ± 98	–	–	1942 ± 51	–	–

The sequence of structural transformations in question is well illustrated by microhardness measurements on cross-sectional fracture surfaces of the samples (Table 2). It follows from these data that, at a given temperature, the hardness of the nitride phase within the forming layers undergoes no significant changes during the nitridation process. The general trend in the variation of microhardness with depth reflects the well-defined graded structure for different process durations (6–60 min). The greatest hardness (from 2200 to 2500 MPa) at each temperature is observed after the completion of the nitridation process, that is, when the composition TiN is reached. The microhardness data for the single-layer samples confirm that they are uniform throughout their cross section.

The measured hardness values correspond to the limiting level for titanium nitride [23] and confirm the above inference that, after high-temperature nitridation, the samples have a heterogeneous structure.

The possibility of a transition from a three-phase to a single-phase structure over a cross section of the samples ensures the formation of both a composite material (with a relatively plastic core and hard shell), which is also reflected in a cross-sectional fracture surface of the sample (Fig. 3), and a coarse-grained titanium nitride-based ceramic.

CONCLUSIONS

The nitridation of rolled titanium is characterized by a sequence of structural changes which reflect the formation of nitride phases differing in composition in the nitrogen diffusion direction. The final stage of the synthesis process yields a nitride close in composition to TiN.

The nitridation process may yield composites in the form of a $TiN/TiN_x/\alpha\text{-}Ti\langle N\rangle$ heterostructure or single-phase, compact titanium nitride-based ceramics, depending on the process duration.

ACKNOWLEDGMENTS

This work was supported by the Russian Science Foundation, project no. 14-13-00925 (federal state budget funded science institution Baikov Institute of Metallurgy and Materials Science, Russian Academy of Sciences).

REFERENCES

1. *Titanium in Medicine: Material Science, Surface Science, Engineering, Biological Responses and Medical Applications,* Brunette, D.M., Ed., New York: Springer, 2001.
2. Cyster, L.A., Grant, D.M., Parker, K.G., and Parker, T.L., The effect of surface chemistry and structure of titanium nitride (TiN) films on primary hippocampal cells, *Biomol. Eng.,* 2002, vol. 19, pp. 171–175.
3. Tribology of Engineered Surfaces, in *Wear Materials, Mechanisms and Practice, Stachowiak, G.W.*, New York: Wiley, 2005.
4. Toth, L.E., *Transition Metal Carbides and Nitrides,* New York: Academic, 1971.
5. Kiuchi, M., Tomita, M., Fujii, K., Satou, M., and Shimizu, R., Titanium nitride crystal growth with preferred orientation by dynamic mixing method, *Jpn. J. Appl. Phys.,* 1987, vol. 26, no. 6, pp. L938–L940.
6. Ingo, G.M., Kaciulis, S., Mezzi, A., Valente, T., Casadei, F., and Gusmanoa, G., Characterization of composite titanium nitride coatings prepared by reactive plasma spraying, *Electrochim. Acta,* 2005, vol. 50, pp. 4531–4537.
7. Danek, M., Liao, M., Tseng, J., Littau, K., Saigal, D., Zhang, H., Mosely, R., and Eizenberg, M., Resistivity reduction and chemical stabilization of organometallic chemical vapor deposited titanium nitride by nitrogen of plasma, *Appl. Phys. Lett.,* 1996, vol. 68, no. 7, pp. 1015–1016.
8. Fix, R.M., Gordon, R.G., and Hoffman, D.M., Synthesis of films by atmospheric pressure chemical vapor deposition using amido and imido titanium(IV) compounds as precursors, *Chem. Mater.,* 1990, vol. 2, pp. 235–241.
9. Bendavid, A., Martin, P.J., Wang, X., Wittling, M., and Kinder, T.J., Deposition and modification of titanium nitride by ion assisted arc deposition, *J. Vac. Sci. Technol., A,* 1995, vol. 13, pp. 1658–1664.
10. Calka, A., Formation of titanium and zirconium nitrides by mechanical alloying, *Appl. Phys. Lett.,* 1991, vol. 59, no. 13, pp. 1568–1569.
11. Castro, D.T. and Ying, J.Y., Synthesis and sintering of nanocrystalline titanium nitride, *Nanostruct. Mater.,* 1997, vol. 9, pp. 67–70.
12. Shin, D.H., Hong, Y.C., and Uhm, H.S., Production of nanocrystalline titanium nitride powder by atmospheric microwave plasma torch in hydrogen/nitrogen gas, *J. Am. Ceram. Soc.,* 2005, vol. 88, no. 10, pp. 2736–2739.
13. Marin-Ayral, R.M., Pascal, C., Martinez, F., and Tedenac, J.C., Simultaneous synthesis and densification of titanium nitride by high pressure combustion synthesis, *J. Eur. Ceram. Soc.,* 2000, vol. 20, pp. 2679–2684.
14. Yang, X., Li, C., Yang, L., Yan, Y., and Qian, Y., Reduction-nitridation synthesis of titanium nitride nanocrystals, *J. Am. Ceram. Soc.,* 2003, vol. 86, no. 1, pp. 206–208.
15. Ramanuja, N., Levy, R.A., Dharmadhikari, S.N., Ramos, E., Pearce, C.W., Menasian, S.C., Schamberger, P.C., and Collins, C.C., Synthesis and characterization of low pressure chemically vapor deposited titanium nitride films using $TiCl_4$ and NH_3, *Mater. Lett.,* 2002, vol. 57, pp. 261–269.
16. Fix, R.M., Gordon, R.G., and Hoffman, D.M., Synthesis of thin films by atmospheric pressure chemical

vapor deposition using amido and imido titanium(IV) compounds as precursors, *Chem. Mater.,* 1990, vol. 2, pp. 235–241.

17. Kuznetsov, K.B., Solntsev, K.A., and Chernyavskii, A.S., RF Patent 2 337 058, 2008.
18. *Diagrammy sostoyaniya dvoinykh metallicheskikh sistem. Spravochnik* (Phase Diagrams of Binary Metallic Systems: A Handbook), Lyakishev, N.P., Ed., Moscow: Mashinostroenie, 1996
19. Kovalev, I.A., Kuznetsov, K.B., Zufman, V.Yu., Ogarkov, A.I., Shevtsov, S.V., Kannykin, S.V., Chernyavskii, A.S., and Solntsev, K.A., High-temperature titanium nitridation kinetics, *Inorg. Mater.,* 2016, vol. 52, no. 12, pp. 1230–1234.
20. Pecharsky, V.K. and Zavalij, P.Y., *Fundamentals of Powder Diffraction and Structural Characterization of Materials,* Berlin: Springer, 2009.
21. Petříček, V., Dušek, M., and Palatinus, L., Crystallographic computing system JANA2006: general features, *Z. Kristallogr.,* 2014, vol. 229, no. 5, pp. 345–352.
22. Höche, D. Schikora, H., et al., Tin-coating formation by pulsed Nd:YAG laser irradiation of titanium in nitrogen, *J. Coat. Technol. Res.,* 2008, vol. 5, no. 14, pp. 505–512.
23. Samsonov, G.V., *Nitridy* (Nitrides), Kiev: Naukova Dumka, 1969.

Translated by O. Tsarev